A study on the nighttime midlatitude ionospheric trough

Maosheng He,[1,2] Libo Liu,[1] Weixing Wan,[1] and Biqiang Zhao[1]

Received 28 October 2010; revised 23 February 2011; accepted 4 March 2011; published 17 May 2011.

[1] Constellation Observing System for Meteorology, Ionosphere, and Climate (COSMIC) electron density profiles are used to investigate the nighttime midlatitude ionospheric trough (MIT). We find that at midnight the longitudinally deepest MIT occurs to the west of the geomagnetic pole in both the Northern and Southern Hemispheres during the equinox seasons and local summer. The deepest MIT could be ascribable to the enhanced depletion caused by horizontal neutral wind. In the early evening, the eastward neutral wind prevails in the midlatitude *F* region, which blows the plasma downward where the declination is eastward in the Northern Hemisphere but westward in the Southern Hemisphere, both lying to the west of the geomagnetic pole. The downward drift would enhance the plasma depletion for more molecular composition at lower altitude. In addition, we find for the first time that the location of nighttime MIT minimum oscillated with a periodicity of 9 days and an amplitude of about 1°–1.5° geomagnetic latitude during 2007–2008, associated with the recurrent high-speed solar wind. Our results shed new light on the empirical description and numerical simulation of MIT.

Citation: He, M., L. Liu, W. Wan, and B. Zhao (2011), A study on the nighttime midlatitude ionospheric trough, *J. Geophys. Res.*, *116*, A05315, doi:10.1029/2010JA016252.

1. Introduction

[2] Longitudinally extended and latitudinally limited regions of depleted plasma density in the ionosphere are termed ionospheric trough (or ionization trough). Troughs show large diversity in their shape and spatial-temporal occurrence, so termed variously according to different characters [*Moffett and Quegan*, 1983; *Rodger et al.*, 1992; *Scali*, 1992]. For example, there is a distinction between the "light-ion trough" and "*F* region trough": the former is characterized by depletions of light ion (H^+, He^+) densities, while the latter reflects mainly the O^+ ion density depletion. Troughs are also termed by the appearing location, such as the daytime trough, predusk trough, dawn trough, midlatitude trough, and high-latitude troughs. Traditionally, troughs found within the auroral oval or in the polar cap are named high-latitude trough, while those observed at latitudes a few degrees lower than the auroral oval are termed midlatitude trough (also called main ionospheric trough, MIT for short) [*Rodger et al.*, 1992].

[3] MIT comprises phenomenologically three elements, the equatorward and the poleward edges separated by the trough minimum. Various mechanisms have been proposed to explain the origin of the elements, which could be roughly divided into two categories. The first subset focuses on the depletion at trough minimum. In the stagnation mechanism, the trough minimum results from the residence in a dark region where the corotation with the Earth and the polar convection counteract each other [*Knudsen*, 1974]. This hypothesis was documented by the results of simulation and observation that the plasma-flowing direction was found to be opposite at the two flanks of premidnight trough. In Sun-Earth reference frame, plasma drifts eastward slowly in the equatorward portion but westward in the poleward portion [*Spiro et al.*, 1978; *Collis and Häggström*, 1988]. Another mechanism, involved principally during geomagnetically active periods, is associated with the electric-field-induced rapid ion drifts, known as polarization jet, subauroral ion drift, substorm-associated auroral surges, and subauroral polarization streams [*Spiro et al.*, 1979; *Anderson et al.*, 1991; *Freeman et al.*, 1992; *Foster and Burke*, 2002; *Galand et al.*, 2002]. The rapid ion drifts could induce a MIT depletion by enhancing the recombination through either nonlinear processes that appear during increases of the relative speeds of the ions to neutrals or the Joule-heating-induced increases in molecular concentration [*Banks et al.*, 1974; *Schunk et al.*, 1975; *Pintér et al.*, 2006; *Rodger*, 2008; *Pirog et al.*, 2009]. In addition, the convection and rapid drift could transport nightside plasma with low concentration into the dayside ionosphere, potentially forming a trough at dayside [*Whalen*, 1989; *Rodger et al.*, 1992; *Mallis and Essex*, 1993; *Pryse et al.*, 1998].

[4] In the above mechanisms, the formation of trough minimum is considered as the dynamic factor, and the equatorward and poleward gradients could be considered as a transition from the minimum depletion to "normal" ionosphere. Besides, there are mechanisms proposed independently to explain the MIT edges, in which the processes

[1]Beijing National Observatory of Space Environment, Institute of Geology and Geophysics, Chinese Academy of Sciences, Beijing, China.
[2]College of Earth Science, Graduate University of Chinese Academy of Sciences, Beijing, China.

0148-0227/11/2010JA016252

in the edges are considered as dynamic factors for MIT generation. The poleward edge of MIT in the evening sector was observed in numerous investigations to colocate with the energetic electron precipitation boundary, so the precipitation was proposed as one of the main source of electrons in the MIT poleward edge in the evening sector [*Turunen and Liszka*, 1972; *St.-Maurice and Torr*, 1978; *Rino et al.*, 1983; *Rodger et al.*, 1986; *Jones et al.*, 1997; *Aladjev et al.*, 2001; *Voiculescu et al.*, 2010]. The gradient at MIT equatorward edge was suggested to be the ionospheric footprint of the plasmapause; at the equator side of the plasmapause the nighttime *F* region is maintained by the plasmasphere, but the maintenance was absent at the pole side of the plasmapause [*Schunk and Banks*, 1975, and references therein]. Consequently, a MIT minimum could be flanked by the plasmasphere-maintaining ionosphere and the precipitation-maintaining. The minimum could be sharpened by the ionization escape along open geomagnetic field lines or/and enhancing recombination due to molecular composition transported by neutral winds or diffusion from aurora oval [*Nishida*, 1967; *Schunk and Banks*, 1975]. It is notable that although the alliance between the equatorward edge and plasmapause was detected by diverse techniques [e.g., *Yizengaw and Moldwin*, 2005; *Yizengaw et al.*, 2005], the alliance breaks down sometimes, for instance, during the storm recovery period [e.g., *Rodger*, 2008].

[5] In the past decades, various ground- and space-based techniques were employed in numerous MIT investigations, so the general morphology and occurrence probability are reasonably well known [*Moffett and Quegan*, 1983; *Rodger et al.*, 1992; *Scali*, 1992]. Globally, the MIT occurs primarily in darkness; thus is observed most regularly in winter (November, December, January, and February for the Northern Hemisphere and May, June, July, and August for the Southern Hemisphere) and equinox; in summer it is restricted mainly to the midnight sector [e.g., *Rodger et al.*, 1992; *Voiculescu et al.*, 2006]. Locally, higher incidences at daytime than nighttime was also reported [*Mallis and Essex*, 1993]. The MIT moves equatorward with increasing geomagnetic activity [*Spiro*, 1978; *Dudeney et al.*, 1983; *Pryse et al.*, 2006]. Local time also affects the MIT location. It moves equatorward with local time in the evening sector, reaches its lowest latitude around midnight and returns to higher latitudes before dawn [*Evans*, 1977; *Whalen*, 1989; *Werner and Prölss*, 1997; *Voiculescu et al.*, 2006]. Numerous publications on the MIT climatology have been reviewed for times [*Evans*, 1977; *Spiro*, 1978; *Prölss*, 2007; *Rodger*, 2008; *Krankowski et al.*, 2009], so MIT's relationships to season, local time and geomagnetic activity are well established. However, the longitudinal dependence has not been comprehensively investigated, probably because previous studies were mainly based on single-pass satellite observations or regional measurements. By a numerical simulation, *Sojka and Schunk* [1989] found the MIT greater extent in zonal direction when the geomagnetic pole is at its farthest from the Sun, 1700 Universal Time (UT) in the Southern Hemisphere and 0500 UT in the Northern Hemisphere. Using TOPEX total electron content (TEC) data, *Horvath and Essex* [2003a] investigated the MIT longitudinal variation and ascribed the longitudinal difference to geomagnetic field intensity, geomagnetic declination and solar insulation. However, they failed to explain how the declination caused the longitudinal variation. In addition, that study was restricted to the southern MIT between 0° and 250°E, because the TOPEX measured TEC just over ocean between 66°N and 66°S.

[6] The huge number of electron density profiles, retrieved from Global Positioning System (GPS) radio occultation (RO) observations of the Constellation Observing System for Meteorology, Ionosphere, and Climate (COSMIC), provided a rich field for investigating the *F* region MIT. The primary purpose of the present work is to extract the peak density and its height (N_mF2 and h_mF2) from COSMIC measurements to study the longitudinal dependence of MIT and its dynamics on a global scale. Besides, multiday periodic oscillations were found in geomagnetic activity and other properties of the Earth's upper atmosphere and inner magnetosphere during the descending and minimum phase of solar cycle 23 [e.g., *Crowley et al.*, 2008; *Lei et al.*, 2008a, 2008b, 2008c; *Liu et al.*, 2010; *Pedatella and Larson*, 2010]. Since the MIT location varies with geomagnetic activity, our starting hypothesis is that multiday periodic oscillations may also present in the MIT minimum. Another purpose of the present work is to explore the potential MIT's oscillation. After a brief description about the data set in section 2, we present the seasonal and longitudinal variation of MIT during quiet time in sections 3.1 and 3.2, and the periodic oscillations in the MIT in section 3.3.

2. Data

[7] The receiver aboard the low-Earth-orbiting COSMIC satellites measures GPS signals, from which electron density profiles are derived by the RO technique [e.g., *Rocken et al.*, 2000; *Schreiner et al.*, 2007]. The six microsatellites of COSMIC have collected about 2.5×10^6 profiles in total until 1 June 2010, more than 1600 profiles per day on average. The post process data were downloaded from the Website of the COSMIC Data Analysis and Archive Center. In Figure 1, we show the distribution of measurements with date. The number of profiles dropped in 2007, resulting from the adjustment of COSMIC orbits from ~500 km to ~800 km. The red line at the top of Figure 1 indicates daily 10.7 cm solar radio flux ($F10.7$). During this period, the daily value of $F10.7$ varies within a range of 65.1–103.2, with an average of 73.4. The solar activity was at its minimum phase. We fit each density profile with a Chapman-α function [*Rishbeth and Garriott*, 1969], from which the N_mF2 and h_mF2 are determined with a least squares fitting procedure, following the manner of *Lei et al.* [2004, 2005] and *Liu et al.* [2007, 2008]. We discarded some profiles with poor quality, about 5% of the total (the yellow portion in Figure 1), according to the values of the related coefficient between the fitted profiles and original data.

[8] *Yue et al.* [2010] compared the simulated RO retrieval with the "true" electron density, which exhibited the correlation between the "true" and retrieved N_mF2 is about 0.95. Some studies [e.g., *Lei et al.*, 2007] had indicated the consistent climatology between the RO observation and traditional techniques. In the present work, TOPEX/Jason total electron content (TEC) and CHAMP in situ electron density are employed to compare with the COSMIC results. Additionally, the magnetic inclination and declination in the present work are calculated from the 10th generation Inter-

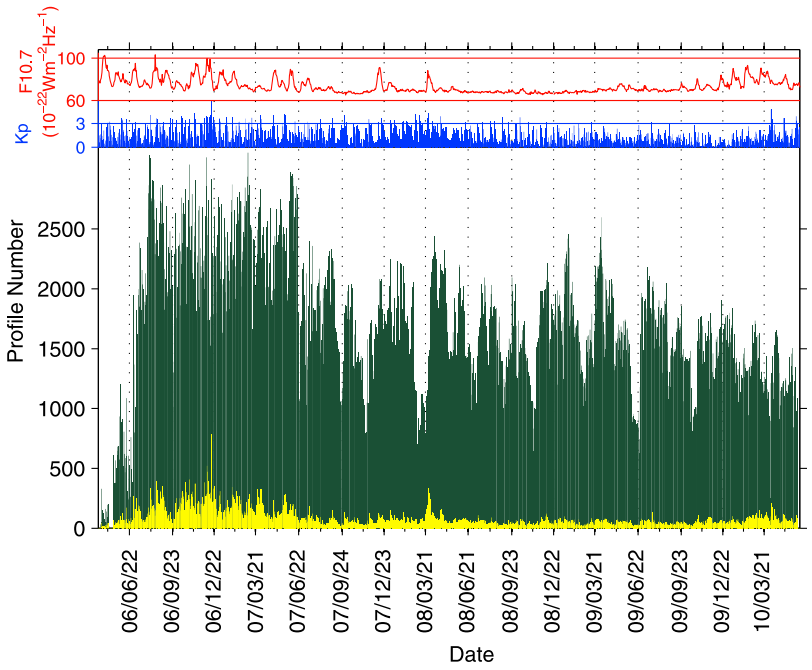

Figure 1. COSMIC profile number as a function of date. The yellow portion is discarded in the present work. The blue bars and red line on the top show daily mean *Kp* index and *F*10.7 index.

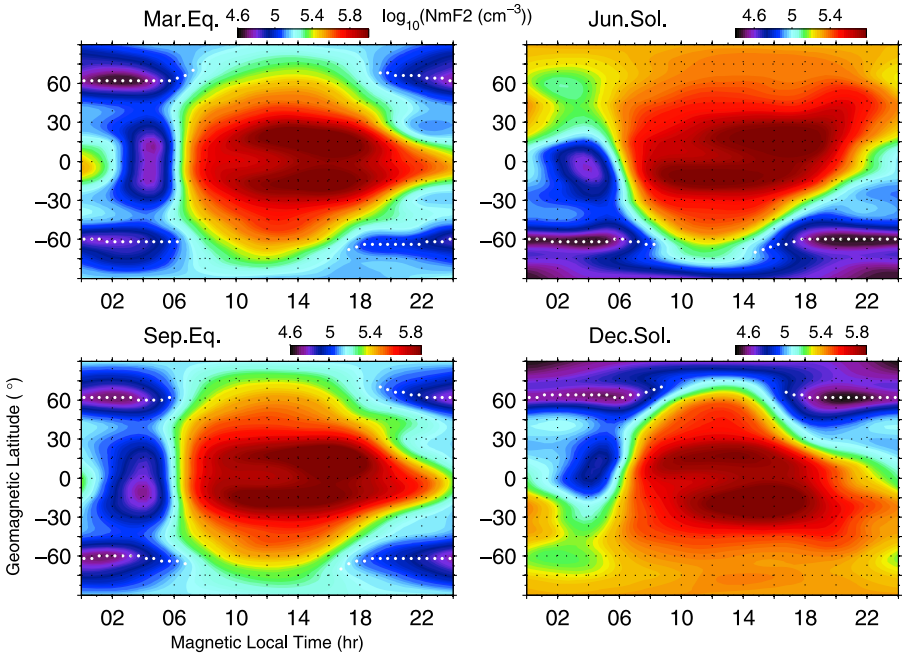

Figure 2. Longitudinally averaged N_mF2 as a function of MLT and geomagnetic latitude under geomagnetically quiet conditions ($Kp < 3$) for the four seasons. To construct the plots, COSMIC data from 2006 to 2010 are binned into four 31 day wide date grids centering on equinoxes and solstices. Dotted lines indicate the typically developed MIT. See the text for details.

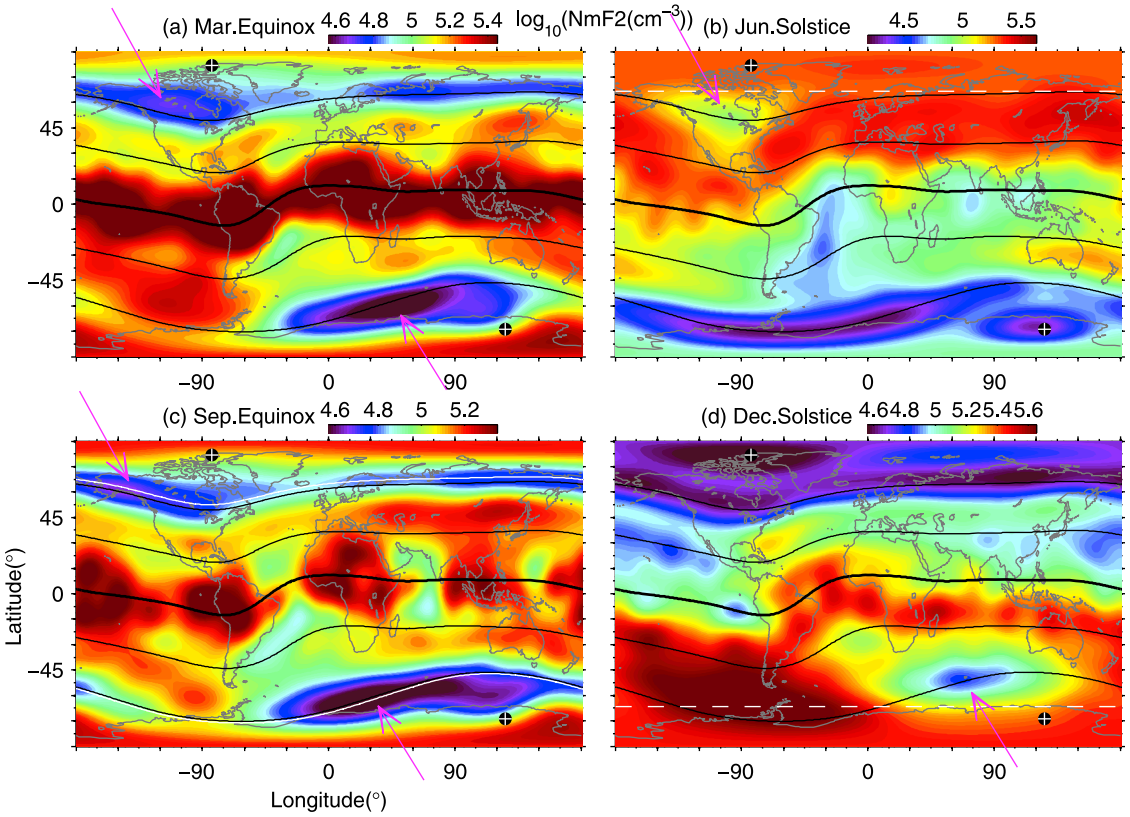

Figure 3. Global maps of COSMIC N_mF2 at midnight (2200–0200 MLT) during geomagnetically quiet periods ($Kp < 3$) for the four seasons. In each map, white crosses on black dots stand for the geomagnetic poles; solid lines show contours of geomagnetic latitudes from 60°N to 60°S with an interval of 20°; and the magenta arrows indicate the longitudinally deepest trough. The dashed lines in Figures 3b and 3d indicate the line where solar zenith angle equals 90° at 0000 LT.

national Geomagnetic Reference Field model (IGRF-10, obtained from the NGDC website).

3. Results and Discussion

3.1. Local Time Dependence

[9] Figure 2 shows the N_mF2 in the frame of magnetic local time (MLT) versus geomagnetic latitude during geomagnetically quiet periods ($Kp < 3$). The COSMIC measurements from 2006 to 2010 are binned into four 31 day wide date grids, centering on the equinoxes and solstices, to represent the four seasons. For each season, a map is constructed by splitting each MLT-latitude cell, with a resolution of 0.5 h by 2° latitude, into a triangle and applying a linear interpolation inside each triangle. A prominent structure elongating in MLT direction is the MIT depletion around the ±60°–70° latitudes. As indicated by the white dotted lines in Figure 2, the MIT extends primarily in darkness, and persists longer in the local winter from ~1600 to ~0800 MLT than at equinoxes from ~1800 to ~0600 MLT, which is consistent with the previous modeling results [*Sojka and Schunk*, 1989]. Besides, the MIT location varies with MLT, primarily at ±60°–62° around midnight, and about ±66°–70° around dusk and dawn, which agrees with the observations of in situ electron density [*Moffett and Quegan*, 1983; *Karpachev et al.*, 1996; *Prölss*, 2007] and GPS TEC [*Wielgosz et al.*, 2004]. The above results demonstrate that the MIT could be observed regularly at nighttime from the COSMIC data. Thus, we study only the nighttime MIT in the following study.

3.2. Longitudinal Dependence

3.2.1. Longitudinal Variations at Midnight

[10] To study the longitudinal variations, we plot in Figure 3 the global N_mF2 maps at midnight for the four seasons under geomagnetically quiet conditions ($Kp < 3$). The N_mF2 measurements collected between 2200 and 0200 MLT are selected, and separated into four seasons as done in section 3.1. For each season, we fit the coefficients of the associated Legendre polynomials from order 0 to order 15. Then N_mF2 is computed by summing the Legendre polynomials at grids with a resolution of 2° longitude by 1° latitude.

[11] Generally, in all the four seasons the N_mF2 is well-aligned with the contours of geomagnetic latitude and the MIT minimum aligns well with the geomagnetic latitude of about ±62°. Two distinct longitudinal variations are the wave number 4 structure [*Wan et al.*, 2008; *He et al.*, 2010] at low latitudes in Figure 3c and the drastic difference along the −60° geomagnetic latitude in Figures 3a, 3c, and 3d. In the summer Southern Hemisphere (Figure 3d), no MIT can be readily found in 180°W–0° where the geomagnetic parallel lies most geographically poleward. This results from

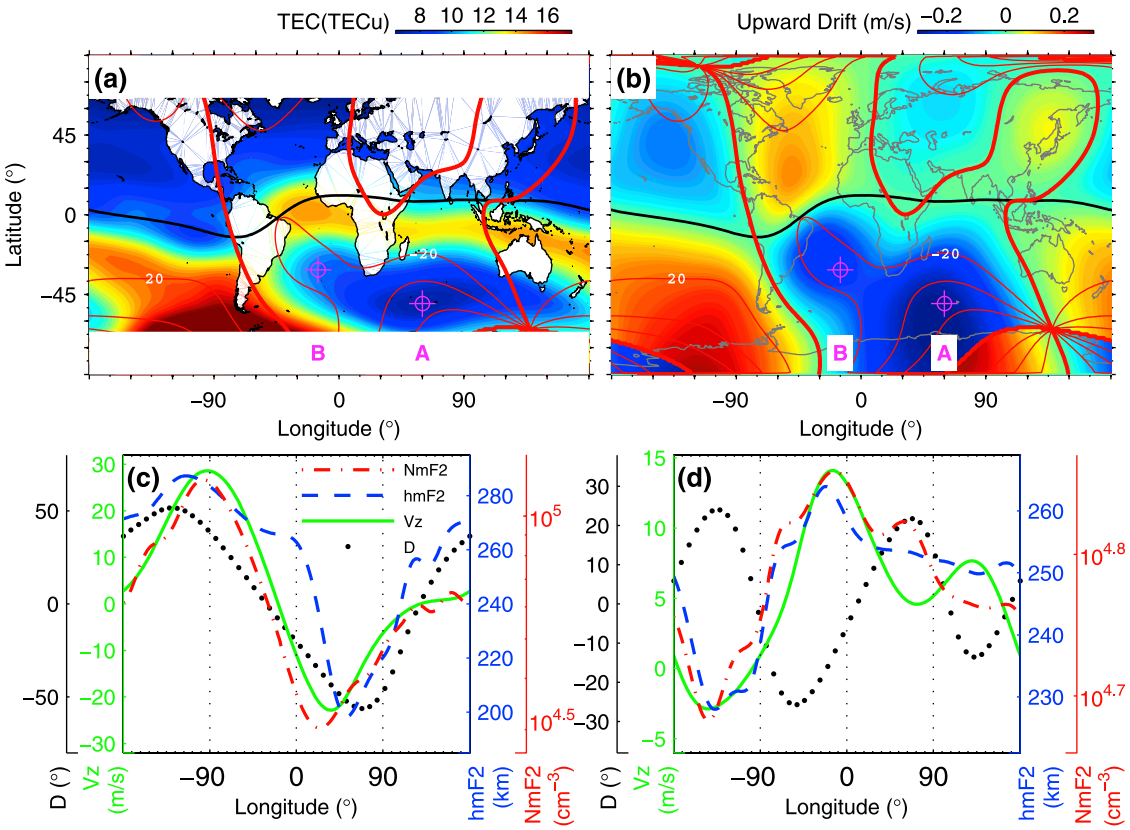

Figure 4. Global maps for (a) TOPEX TEC at the December solstice for midnight quiet conditions at low solar activity minimum (2200–0200 MLT, $Kp < 3$, $F10.7 < 100$) and (b) vertical drift induced by the eastward wind at a speed of 1 m/s. (c) Longitudinal variation of the declination (the dotted line) at southern MIT minimum (on the southern white line in Figure 3c), along with those of wind-induced vertical drift in the early evening (the solid line), h_mF2 in the late evening (the dashed line), and N_mF2 at midnight (the dash-dotted line). (d) The same as Figure 4c but along the northern white line in Figure 3c. In Figures 4a and 4b the red solid lines indicate declination contours with a 20° interval, and the black lines show the geomagnetic equator. In Figures 4c and 4d the geomagnetic components are calculated from the tenth-generation International Geomagnetic Reference Field model (IGRF-10); Vz is calculated according to the Horizontal Wind Model (HWM07), at 1900 LT September equinox, $F10.7 = 70$; and the h_mF2 and N_mF2 curves are fitted with Legendre polynomials on the COSMIC measurements collected in 2200–2400 and 2200–0200 MLT, respectively, at the September equinox under geomagnetically quiet conditions ($Kp < 3$).

the dependence of MIT occurrence on illuminating condition [*Sharp*, 1966; *Spiro*, 1978; *Karpachev*, 2003]. In the longitude sector where the southern trough disappears, there is permanent insolation at −62° geomagnetic latitude (the mean latitude of MIT) at summer solstice, which prevents trough formation. The white line in Figure 3d indicates the terminator at 0000 LT; it can be found that the contour line of −60° geomagnetic latitude between 135°W and 15°E is on the sunlit side. Actually, N_mF2 is increasing in the permanently illuminated region in the summer evening, known as the Weddell Sea Anomaly [*Horvath and Essex*, 2003b; *Horvath*, 2006; *Burns et al.*, 2008; *He et al.*, 2009]. Contrarily, in the longitude sector close to the geographic longitude of the geomagnetic pole, the contour line of −60° geomagnetic latitude lies in the darkness at summer midnight, and MIT occurs there. The illuminating condition could explain the general features of the longitudinal difference. However, Figure 3d shows that the southern MIT develops deepest in 60°–75°E (indicated by the magenta arrow), rather than at ~125°E, where the MIT locates lowest latitude and stays longest in darkness. At equinoxes, the southern MIT minimum is deepest at 15°–75°E, as well to the west of the longitude of the geomagnetic pole.

[12] In the Northern Hemisphere, the contour lines of geomagnetic latitude lie most geographically poleward between 0° and 180°E where the MIT can hardly be found in summer (Figure 3b) owing to the lasting illumination as well. Besides, the deepest MIT develops in 105°–75°W during summer (denoted by the arrow in Figure 3b) and in 180°–90°W at equinoxes (Figures 3a and 3c), both of which lie to the west of the northern geomagnetic pole.

3.2.2. Thermospheric Wind Effect

[13] We have shown above the longitudinal variations of midnight MIT for the four seasons. In both the equinox seasons and local summer, N_mF2 at the trough minimum varies with longitude; it minimizes in the longitude sector to

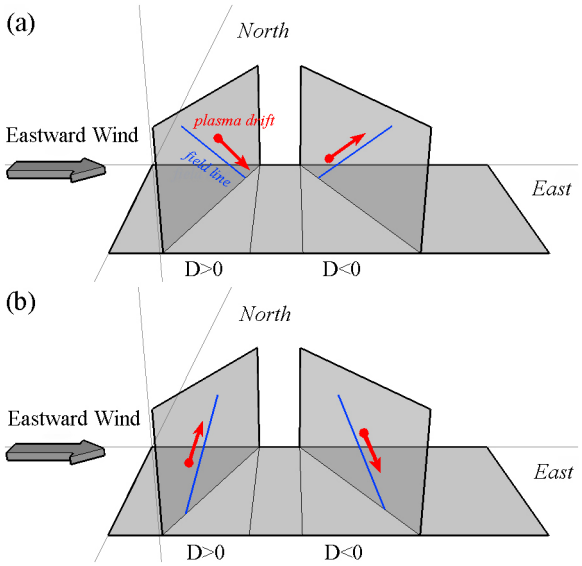

Figure 5. Eastward-wind-induced vertical drift in (a) the Northern Hemisphere and (b) the Southern Hemisphere.

the west of geomagnetic pole in both the Northern and Southern Hemisphere. In order to confirm the COSMIC observations reflect what is really happening, we carry on a comparison in Figure 4a, a global TOPEX/Jason TEC map at December solstice midnight under solar minimum, geomagnetically quiet conditions ($F10.7 < 100$, $Kp < 3$) collected between 1993 and 2008. The MIT in TEC is deepest around 50°S, 60°E as well (marked as Point A in Figure 4a) similar to that in the previous N_mF2 map (Figure 3d). Besides, in Figure 4a the deepest MIT depletion seems to spread equatorward toward the Point B (15°W, 31°S), in the direction of the −20° magnetic declination shifting equatorward. The equatorward spreading depletion can also be found in N_mF2 (Figure 3d).

[14] A physical process associated with declination is the vertical drift induced by horizontal neutral wind. In the F region, the effective upward drift velocity of plasma induced by the horizontal wind with northward and eastward speed components W_{north} and W_{east} is

$$V_z = W_{\text{Mnorth}}/2 \cdot \sin(2I), W_{\text{Mnorth}} = W_{\text{north}} \cdot \cos(D) + W_{\text{east}} \cdot \sin(D). \quad (1)$$

Here I is the magnetic dip angle, D is the magnetic declination, and W_{Mnorth} is the northward component of wind in the magnetic meridian [*He et al.*, 2009]. The geometry of the magnetic field would cause a considerable horizontal gradient in plasma vertical drift. W_{east} reaches its diurnal maximum in the early evening while the magnitude of W_{north} is at its minimum, according to theoretical simulation [*Dickinson et al.*, 1981], empirical models [*Hedin et al.*, 1988, 1991; *Titheridge*, 1995], or direct measurements [*Emmert et al.*, 2003, 2006]. Figure 4b presents the global vertical drift induced by eastward wind at the speed of 1 m/s; the vertical drift varies with the declination, especially at midlatitudes. In the Southern Hemisphere plasma would be blown upward where declination is positive (eastward) but downward where the declination is negative. The downward drift peaks at the midlatitudes around 60°E where the −40° to −60° contour lines of the declination protrude equatorward. As in the servo manner [*Rishbeth*, 1967, 1968], upward (downward) drift would rise (fall) the $F2$ peak and further increase (decrease) N_mF2 for less recombination at higher altitude.

[15] As an example to illustrate the wind effect, the solid line in Figure 4c indicates the longitudinal variation of the wind-induced vertical drift at the southern MIT minimum, according to the Horizontal Wind Model (HWM07) [*Drob et al.*, 2008]. The vertical drift is calculated at 250 km altitude after sunset (1900 LT) at September equinox on the southern white line in Figure 3c. The upward drift maximizes at 29 m/s in 120°–90° W where the declination is eastward, and minimizes at −23 m/s in 0°–60° E where the declination is westward. The dashed line in Figure 4c indicates the COSMIC h_mF2 at 2200–2400 MLT on the southern white line in Figure 3c, which also peaks at 120°–90° W and valleys at 0°–60° E. After sunset, the ionospheric plasma deplete gradually in darkness. The time constant of plasma, proportional to $1/\beta$, increases exponentially with altitudes. In consequence, the decaying rate of N_mF2 would increase with decreasing h_mF2, which could result in the longitudinal N_mF2 variation at midnight (the dash-dotted line in Figure 4c). The valleys of the curves do not locate exactly at the same longitude, because the peak height does not response immediately to winds for its cumulative nature [*Bailey et al.*, 1997], and N_mF2 cannot react immediately to the change in h_mF2 because plasma take time to deplete [e.g., *Bauske and Prölss*, 1997; *Prölss and Ocko*, 2000].

[16] In the Northern Hemisphere, the dependence of eastward-winds-induced vertical drift on the declination is opposite to that in the Southern Hemisphere, as indicated in the sketch in Figure 5. Hence, contrary to the Southern Hemisphere, the downward drift appears where the declination is positive in the Northern Hemisphere. Figure 4d is the same plot as Figure 4c but along the northern white line in Figure 3c. The h_mF2 and N_mF2 in Figure 4d depend less on wind-induced vertical drift compared with that in Figure 4c, because the vertical drift is smaller in the Northern Hemisphere and other processes such as electric-field-induced vertical drift can be as significant as the wind effect. Nonetheless, in Figure 4d all three curves peak in 60°–30°W and valley in 160°–130°W.

[17] In winter, the effect of winds on the longitudinal variation is less significant than the effect from illuminating condition. The longitudinally deepest MIT occurs at ~110°E in the Northern Hemisphere (Figure 3b) and 100°W–0° in the Southern Hemisphere (Figure 3d), both of which are in the longitude sector where the MIT locates at its highest geographic latitude and in permanent darkness at winter solstice.

3.3. Multiday Oscillation

[18] Recently, increasing attentions have been paid on 9 day periodic oscillations in properties of terrestrial space, such as thermospheric parameters and plasmapause location during the deep solar minimum of solar cycles 23/24 [*Gibson et al.*, 2009; *Lei et al.*, 2010; *Pedatella and Larson*, 2010; *Pedatella et al.*, 2010]. Since it is well known that the MIT minimum moves equatorward (poleward) with

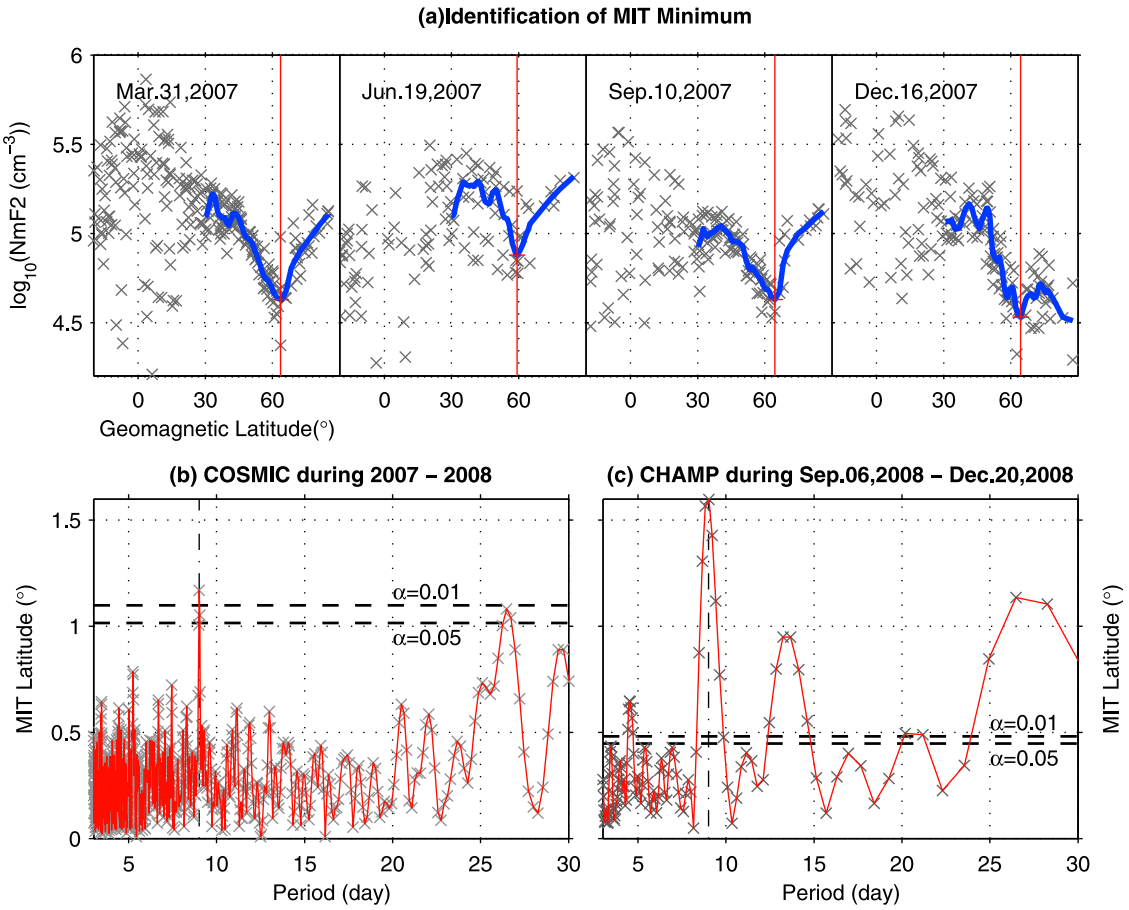

Figure 6. (a) Examples of MIT identification from daily COSMIC radio occultation observations. The blue lines show the average of the scatter crosses in 10° latitude wide sliding windows, and the red lines indicate the positions of MIT minimum. (b) Lomb-Scargle periodograms of the COSMIC-measured latitude of MIT minimum at nighttime during 2007–2008. (c) Same as Figure 6b but measured by CHAMP during 6 September 2008 to 20 December 2008. The horizontal dashed lines in Figures 6b and 6c indicate the significance levels of 0.05 and 0.01. See the text for details.

increasing (decreasing) geomagnetic levels [e.g., *Rycroft and Burnell*, 1970; *Rycroft and Thomas*, 1970; *Lee et al.*, 2010], we investigate whether the periodic oscillation observed in geomagnetic activity produces a detectable signature in MIT location.

[19] We identify a time series of the latitude of MIT minimum from COSMIC observations following the procedure below. First, we herein focus on the northern MIT within 2300–0500 LT sector and within the geomagnetic longitude sector between 100°W and 100°E. The selected longitude sector is rotating with the Earth while the LT sector is stillness in Sun-synchronous frame. Hence, the longitude sector is passing through the LT sector during about −0200–1700 UT every day. Second, N_mF2 measurements are binned day by day, from −0600 UT to 1800 UT for each day. Third, in each bin, we pick out the measurements in the intersection of the two sectors, sort the them by geomagnetic latitude (*Mlat*), average them within a 10° latitude wide sliding window, and get a latitudinal profile $N_mF2(Mlat)$. Finally, the latitude of MIT minimum is identified on $N_mF2(Mlat)$ following the manner of *Prölss* [2007]. Examples of the MIT identifying are shown in Figure 6a.

[20] Following the above procedures, we obtain a series of the latitude of MIT minimum as a function of date. Lomb-Scargle (LS) periodogram [*Lomb*, 1976] is calculated for the series between 2007 and 2008, shown in Figure 6b. The horizontal dashed lines in the periodogram indicate the statistical significance (α = 0.05, 0.01). The α is the probability that the periodicities with the amplitude denoted by the corresponding dashed line have occurred by chance alone. Dominant spectral components above α = 0.05 level are found at 9 and 27 day periods, with amplitudes of 1.2° and 1.1°. We carry on a comparison in Figure 6c, which are the same plots as Figure 6b but identified from in situ electron density measured by CHAMP at ~400 km during 6 September 2008 to 20 December 2008. On 6 September 2008 the descending orbit of CHAMP covered around 0530 LT, precessing to 2000 LT on 20 December 2008. In Figure 6c, the most remarkable component is observed at a 9 day period with amplitude of 1.6°. The COSMIC spectrum differs from the CHAMP at several aspects. For example, the components in Figure 6b are generally less significant than those in Figure 6c. Two factors account primarily for the differences. First, the sampling frequency and scope are

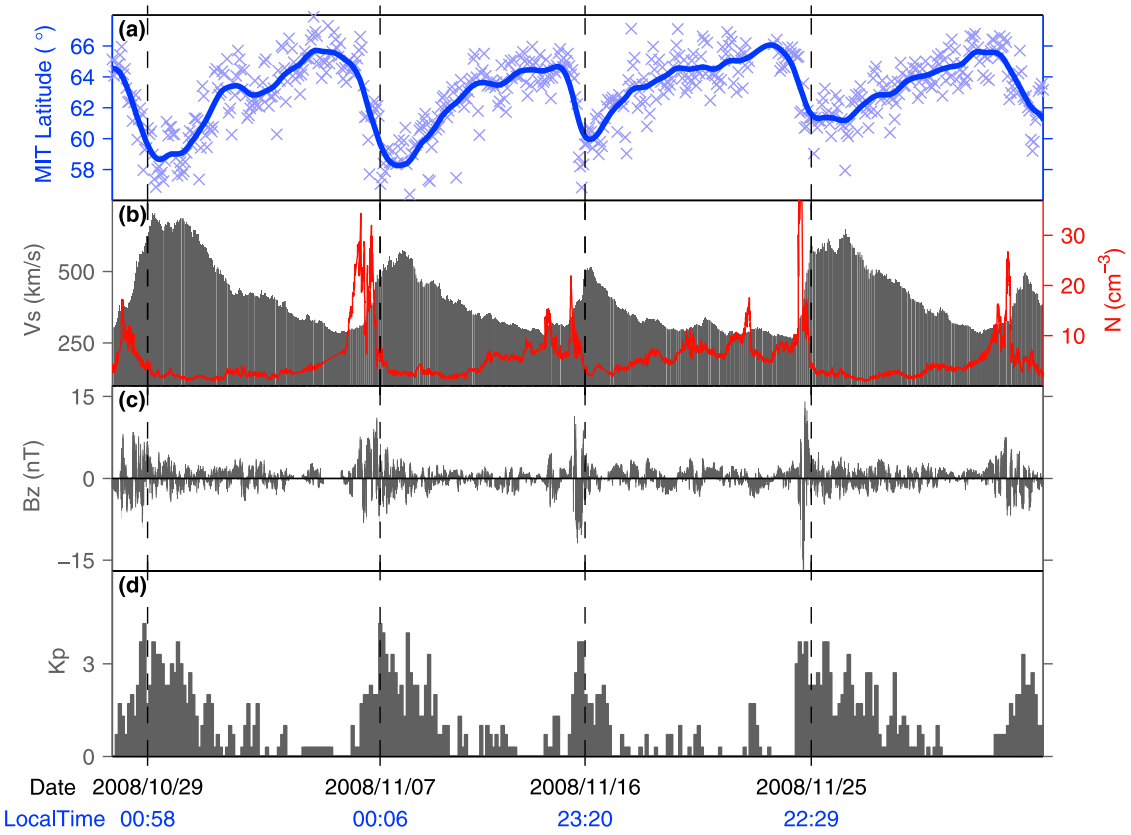

Figure 7. (a) The CHAMP-measured latitude of MIT minimum around midnight during 28 October 2008 to 5 December 2008, along with (b) solar wind speed *V*s and solar wind proton density *N*, (c) interplanetary magnetic field *B*z, and (d) *Kp* index. The solid line in Figure 6a indicates the cubic smoothing spline for the scatter crosses. See the text for details.

different. The COSMIC series is sampled from 1 June 2007 to 31 December 2008 with an interval of 1 day while the CHAMP from 6 September 2008 to 20 December 2008 with an interval of ~1.6 h. The other is the spatial and temporal resolution. The resolution of COSMIC MIT is 200° in longitude, ~18 h in UT span, and 6 h in LT, while the CHAMP MIT is measured in situ and transient. Hence, the COSMIC data are ineffective in demonstrating the details in the MIT periodogram; for example, the 13.5 day component found in Figure 6c can hardly be found in Figure 6b.

[21] To examine the MIT oscillation in detail, we show in Figure 7a a time series of the CHAMP-measured MIT latitude between 28 October 2008 and 5 December 2008. The MIT was detected for ~15 times per day, distributing roughly equidistantly in 360° longitudes. The MIT latitudes scattered in Figure 7a are fitted to the solid line by using a cubic smoothing spline. The range from the peak to valley on the smoothed line is about 6°–7°. Figures 7b–7d contain the solar wind speed *V*s with solar wind proton density *N*, interplanetary magnetic field *B*z, and *Kp* index, respectively. In Figure 7, the correlation coefficient (r_{Vs}) between *V*s and the smoothed MIT latitude is −0.86 at significance level (α_{Vs}) of 1.68×10^{-273}. For comparison, $r_{Kp} = -0.74$ at $\alpha_{Kp} = 2.23 \times 10^{-53}$, $r_{AE} = -0.63$ at $\alpha_{AE} = 1.12 \times 10^{-101}$, $r_{Dst} = 0.43$ at $\alpha_{Dst} = 7.46 \times 10^{-42}$. The high correlation between the MIT latitude and solar wind speed supports the conclusions about a link between MIT and solar wind parameters [*Voiculescu et al.*, 2006; *Voiculescu and Nygrén*, 2007].

[22] The multiday oscillations in solar winds speed are believed to arise from the multiple coronal holes distributing on solar disk [e.g., *Temmer et al.*, 2007; *Lei et al.*, 2010]. The coronal hole is region with open magnetic field associated with emission of high-speed stream (HSS) [*Krieger et al.*, 1973]. During the descending phase of solar cycle, the coronal hole elongates to lower latitudes [*Burlaga et al.*, 1978]. Multiple coronal holes fixed at the Sun could produce recurrent HSS as the second (13.5 day) and third (9 day) harmonics of the ~27 day rotation. The recurrent HSS could directly drive an oscillation in MIT. In high-latitude ionosphere, the convection is driven by local electric field ($\boldsymbol{E}_{\mathrm{I}}$). In the Earth's frame, the solar wind's dawn-dusk electric field ($\boldsymbol{E}_{\mathrm{SW}}$) and its speed ($\boldsymbol{V}_{\mathrm{SW}}$) relate by the equation $\boldsymbol{E}_{\mathrm{SW}} = -\boldsymbol{V}_{\mathrm{SW}} \times \boldsymbol{B}$ [*Burton et al.*, 1975]. Accordingly, increase in $\boldsymbol{V}_{\mathrm{SW}}$ would enhance the $\boldsymbol{E}_{\mathrm{SW}}$, which could enhance $\boldsymbol{E}_{\mathrm{I}}$ by mapping along the magnetic field lines downward into ionosphere, further enhancing the $\boldsymbol{E} \times \boldsymbol{B}$ convection and expanding the convection pattern [*Sojka et al.*, 1981; *Khan and Cowley*, 1999]. As a result, the stagnation point and the stagnation MIT would shift equatorward. Besides, the HSS-induced magnetic storm could also account for the MIT's oscillation. In Figure 7b, recurrent HHS are headed by compressed dense solar winds associated with rapid *B*z

oscillations (in Figure 7c) and *Kp* fluctuations (in Figure 7d), which are the typical features of the HSS-induced magnetic storm [*Tsurutani et al.*, 1995, 2006]. The geomagnetic disturbances would expand the auroral boundary to lower latitude [*Akasofu and Chapman*, 1963; *Prölss*, 1995; *Carbary*, 2005], which could shift the aurora-associated MIT equatorward.

4. Conclusions

[23] COSMIC N_mF2 and h_mF2 are utilized to analyze the nighttime midlatitude trough. Our major findings are a longitudinal dependence and a response to solar winds.

[24] 1. In the Southern Hemisphere during the equinox seasons and summer, the midnight deepest trough locates in the 0°–90°E sector, to the west of the geomagnetic pole. Likewise, in the Northern Hemisphere, the midnight deepest MIT occurs in the 150°–90°W sector, to the west of northern geomagnetic pole. The MIT's dependence on the pole location could be explained in terms of the neutral winds and the geometry of the magnetic field. In the midlatitude *F* region, the prevailing neutral winds is eastward in the early evening. The eastward wind would blow the plasma downward where the declination is westward in the Southern Hemisphere but where the declination is eastward in the Northern Hemisphere, both of which lie to the west of respective geomagnetic pole. The downward drift results in the *F*2 peak forming at a lower altitude, enhancing the MIT depletion.

[25] 2. We find the latitude of *F* region MIT fluctuates with a close relationship to the solar wind speed. The latitude of nighttime MIT minimum oscillated at a 9 day period, responding to the periodic appearance of the high-speed solar winds. The high correlation between the MIT latitude and solar wind speed suggests a link between solar winds and MIT, and provides a probability to forecast the fluctuation of MIT location using solar wind parameters.

[26] **Acknowledgments.** M. He thanks J. Lei for his illuminating discussions. The authors thank R. W. Spiro for his kind help. This study used the IRO data from the COSMIC Data Analysis and Archive Center. The *F*10.7 index and magnetic activity *Kp* , *AE*, and *Dst* indexes were also obtained from the NGDC database, and solar wind data were obtained from the GSFC/SPDF OMNIWeb interface, http://omniweb.gsfc.nasa.gov. The TOPEX/Jason TEC were downloaded from the Physical Oceanography DAAC, the JPL ftp server, ftp://podaac.jpl.nasa.gov. The CHAMP in situ electron density data were obtained from the GFZ, http://isdc.gfz-potsdam.de. This research is supported by the National Natural Science Foundation of China (40725014, 41074112).

[27] Robert Lysak thanks Mirela Voiculescu and Alan Rodger for their assistance in evaluating this paper.

References

Akasofu, S. I., and S. Chapman (1963), The lower limit of latitude (US sector) of northern quiet auroral arcs, and its relation to *Dst*(*H*), *J. Atmos. Terr. Phys.*, *25*(1), 9–12, doi:10.1016/0021-9169(63)90011-4.

Aladjev, G. A., O. V. Evstafiev, V. S. Mingalev, G. I. Mingaleva, E. D. Tereshchenko, and B. Z. Khudukon (2001), Interpretation of ionospheric *F*-region structures in the vicinity of ionisation troughs observed by satellite radio tomography, *Ann. Geophys.*, *19*(1), 25–36, doi:10.5194/angeo-19-25-2001.

Anderson, P. C., R. A. Heelis, and W. B. Hanson (1991), The ionospheric signatures of rapid subauroral ion drifts, *J. Geophys. Res.*, *96*(A4), 5785–5792, doi:10.1029/90JA02651.

Bailey, G. J., N. Balan, and Y. Z. Su (1997), The Sheffield Univ. plasmasphere ionosphere model: A review, *J. Atmos. Sol. Terr. Phys.*, *59*(13), 1541–1552, doi:10.1016/S1364-6826(96)00155-1.

Banks, P. M., R. W. Schunk, and W. J. Raitt (1974), NO^+ and O^+ in the high latitude F-region, *Geophys. Res. Lett.*, *1*(6), 239–242, doi:10.1029/GL001i006p00239.

Bauske, R., and G. W. Prölss (1997), Modeling the ionospheric response to traveling atmospheric disturbances, *J. Geophys. Res.*, *102*(A7), 14,555–14,562, doi:10.1029/97JA00941.

Burlaga, L. F., K. W. Behannon, S. F. Hansen, G. W. Pneuman, and W. C. Feldman (1978), Sources of magnetic fields in recurrent interplanetary streams, *J. Geophys. Res.*, *83*(A9), 4177–4185, doi:10.1029/JA083iA09p04177.

Burns, A. G., Z. Zeng, W. Wang, J. Lei, S. C. Solomon, A. D. Richmond, T. L. Killeen, and Y.-H. Kuo (2008), Behavior of the F_2 peak ionosphere over the South Pacific at dusk during quiet summer conditions from COSMIC data, *J. Geophys. Res.*, *113*, A12305, doi:10.1029/2008JA013308.

Burton, R. K., R. L. McPherron, and C. T. Russell (1975), An empirical relationship between interplanetary conditions and *Dst*, *J. Geophys. Res.*, *80*(31), 4204–4214, doi:10.1029/JA080i031p04204.

Carbary, J. F. (2005), A *Kp*-based model of auroral boundaries, *Space Weather*, *3*, S10001, doi:10.1029/2005SW000162.

Collis, P. N., and I. Häggström (1988), Plasma convection and auroral precipitation processes associated with the main ionospheric trough at high latitudes, *J. Atmos. Terr. Phys.*, *50*(4–5), 389–404, doi:10.1016/0021-9169(88)90024-4.

Crowley, G., A. Reynolds, J. P. Thayer, J. Lei, L. J. Paxton, A. B. Christensen, Y. Zhang, R. R. Meier, and D. J. Strickland (2008), Periodic modulations in thermospheric composition by solar wind high speed streams, *Geophys. Res. Lett.*, *35*, L21106, doi:10.1029/2008GL035745.

Dickinson, R. E., E. C. Ridley, and R. G. Roble (1981), A three-dimensional general circulation model of the thermosphere, *J. Geophys. Res.*, *86*(A3), 1499–1512, doi:10.1029/JA086iA03p01499.

Drob, D. P., et al. (2008), An empirical model of the Earth's horizontal wind fields: HWM07, *J. Geophys. Res.*, *113*, A12304, doi:10.1029/2008JA013668.

Dudeney, J. R., A. S. Rodger, and M. J. Jarvis (1983), Radio studies of the main F region trough in Antarctica, *Radio Sci.*, *18*(6), 927–936, doi:10.1029/RS018i006p00927.

Emmert, J. T., B. G. Fejer, and D. P. Sipler (2003), Climatology and latitudinal gradients of quiet time thermospheric neutral winds over Millstone Hill from Fabry-Perot interferometer measurements, *J. Geophys. Res.*, *108*(A5), 1196, doi:10.1029/2002JA009765.

Emmert, J. T., M. L. Faivre, G. Hernandez, M. J. Jarvis, J. W. Meriwether, R. J. Niciejewski, D. P. Sipler, and C. A. Tepley (2006), Climatologies of nighttime upper thermospheric winds measured by ground-based Fabry-Perot interferometers during geomagnetically quiet conditions: 1. Local time, latitudinal, seasonal, and solar cycle dependence, *J. Geophys. Res.*, *111*, A12302, doi:10.1029/2006JA011948.

Evans, J. V. (1977), Satellite beacon contributions to studies of the structure of the ionosphere, *Rev. Geophys.*, *15*(3), 325–350, doi:10.1029/RG015i003p00325.

Foster, J. C., and W. J. Burke (2002), SAPS: A new categorization for subauroral electric fields, *Eos Trans. AGU*, *83*(36), 393, doi:10.1029/2002EO000289.

Freeman, M. P., D. J. Southwood, M. Lester, T. K. Yeoman, and G. D. Reeves (1992), Substorm-associated radar auroral surges, *J. Geophys. Res.*, *97*(A8), 12,173–12,185, doi:10.1029/92JA00697.

Galand, M., D. Lummerzheim, A. W. Stephan, B. C. Bush, and S. Chakrabarti (2002), Electron and proton aurora observed spectroscopically in the far ultraviolet, *J. Geophys. Res.*, *107*(A7), 1129, doi:10.1029/2001JA000235.

Gibson, S. E., J. U. Kozyra, G. de Toma, B. A. Emery, T. Onsager, and B. J. Thompson (2009), If the Sun is so quiet, why is the Earth ringing?: A comparison of two solar minimum intervals, *J. Geophys. Res.*, *114*, A09105, doi:10.1029/2009JA014342.

He, M., L. Liu, W. Wan, B. Ning, B. Zhao, J. Wen, X. Yue, and H. Le (2009), A study of the Weddell Sea Anomaly observed by FORMOSAT-3/COSMIC, *J. Geophys. Res.*, *114*, A12309, doi:10.1029/2009JA014175.

He, M., L. Liu, W. Wan, J. Lei, and B. Zhao (2010), Longitudinal modulation of the O/N2 column density retrieved from TIMED/GUVI measurement, *Geophys. Res. Lett.*, *37*, L20108, doi:10.1029/2010GL045105.

Hedin, A. E., N. W. Spencer, and T. L. Killeen (1988), Empirical global model of upper thermosphere winds based on atmosphere and dynamics explorer satellite data, *J. Geophys. Res.*, *93*(A9), 9959–9978, doi:10.1029/JA093iA09p09959.

Hedin, A. E., et al. (1991), Revised global model of thermosphere winds using satellite and ground-based observations, *J. Geophys. Res.*, *96*(A5), 7657–7688, doi:10.1029/91JA00251.

Horvath, I. (2006), A total electron content space weather study of the nighttime Weddell Sea Anomaly of 1996/1997 southern summer with TOPEX/Poseidon radar altimetry, *J. Geophys. Res.*, *111*, A12317, doi:10.1029/2006JA011679.

Horvath, I., and E. A. Essex (2003a), The southern-hemisphere mid-latitude day-time and night-time trough at low-sunspot numbers, *J. Atmos. Sol. Terr. Phys.*, *65*(8), 917–940, doi:10.1016/S1364-6826(03)00113-5.

Horvath, I., and E. A. Essex (2003b), The Weddell sea anomaly observed with the TOPEX satellite data, *J. Atmos. Sol. Terr. Phys.*, *65*(6), 693–706, doi:10.1016/S1364-6826(03)00083-X.

Jones, D. G., I. K. Walker, and L. Kersley (1997), Structure of the poleward wall of the trough and the inclination of the geomagnetic field above the EISCAT radar, *Ann. Geophys.*, *15*(6), 740–746, doi:10.1007/s00585-997-0740-8.

Karpachev, A. T. (2003), The dependence of the main ionospheric trough shape on longitude, altitude, season, local time, and solar and magnetic activity, *Geomagn. Aeron.*, *43*(2), 239–251.

Karpachev, A. T., M. G. Deminov, and V. V. Afonin (1996), Model of the mid-latitude ionospheric trough on the base of Cosmos-900 and Intercosmos-19 satellites data, *Adv. Space Res.*, *18*(6), 221–230, doi:10.1016/0273-1177(95)00928-0.

Khan, H., and S. W. H. Cowley (1999), Observations of the response time of high-latitude ionospheric convection to variations in the interplanetary magnetic field using EISCAT and IMP-8 data, *Ann. Geophys.*, *17*(10), 1306–1335, doi:10.1007/s00585-999-1306-8.

Knudsen, W. (1974), Magnetospheric convection and the high-latitude F_2 ionosphere, *J. Geophys. Res.*, *79*(7), 1046–1055, doi:10.1029/JA079i007p01046.

Krankowski, A., I. I. Shagimuratov, I. I. Ephishov, A. Krypiak-Gregorczyk, and G. Yakimova (2009), The occurrence of the mid-latitude ionospheric trough in GPS-*TEC* measurements, *Adv. Space Res.*, *43*(11), 1721–1731, doi:10.1016/j.asr.2008.05.014.

Krieger, A. S., A. F. Timothy, and E. C. Roelof (1973), A coronal hole and its identification as the source of a high velocity solar wind stream, *Sol. Phys.*, *29*(2), 505–525, doi:10.1007/BF00150828.

Lee, I., J. Y. Liu, W. Wang, C. Chen, and C. Lin (2010), The ionospheric mid-latitude trough observed by FORMOSAT-3/COSMIC during solar minimum, *Eos Trans. AGU*, *91*(26), West. Pac. Geophys. Meet. Suppl., Abstract SPA44B–02.

Lei, J., L. Liu, W. Wan, S.-R. Zhang, and J. M. Holt (2004), A statistical study of ionospheric profile parameters derived from Millstone Hill incoherent scatter radar measurements, *Geophys. Res. Lett.*, *31*, L14804, doi:10.1029/2004GL020578.

Lei, J., L. Liu, W. Wan, and S.-R. Zhang (2005), Variations of electron density based on long-term incoherent scatter radar and ionosonde measurements over Millstone Hill, *Radio Sci.*, *40*, RS2008, doi:10.1029/2004RS003106.

Lei, J., S. Syndergaard, A. Burns, S. Solomon, W. Wang, Z. Zeng, R. Roble, Q. Wu, Y. Kuo, and J. Holt (2007), Comparison of COSMIC ionospheric measurements with ground-based observations and model predictions: Preliminary results, *J. Geophys. Res.*, *112*, A07308, doi:10.1029/2006JA012240.

Lei, J., J. Thayer, J. Forbes, E. Sutton, and R. Nerem (2008a), Rotating solar coronal holes and periodic modulation of the upper atmosphere, *Geophys. Res. Lett.*, *35*, L10109, doi:10.1029/2008GL033875.

Lei, J., J. P. Thayer, J. M. Forbes, E. K. Sutton, R. S. Nerem, M. Temmer, and A. M. Veronig (2008b), Global thermospheric density variations caused by high-speed solar wind streams during the declining phase of solar cycle 23, *J. Geophys. Res.*, *113*, A11303, doi:10.1029/2008JA013433.

Lei, J., J. P. Thayer, J. M. Forbes, Q. Wu, C. She, W. Wan, and W. Wang (2008c), Ionosphere response to solar wind high-speed streams, *Geophys. Res. Lett.*, *35*, L19105, doi:10.1029/2008GL035208.

Lei, J., J. Thayer, W. Wang, and R. McPherron (2010), Impact of CIR storms on thermosphere density variability during the solar minimum of 2008, *Sol. Phys.*, 1–11, doi:10.1007/s11207-010-9563-y.

Liu, J., L. Liu, B. Zhao, W. Wan, and R. A. Heelis (2010), The responses of the topside ionosphere to recurrent geomagnetic activity, *J. Geophys. Res.*, *115*, A12327, doi:10.1029/2010JA015810.

Liu, L., H. Le, W. Wan, M. Sulzer, J. Lei, and M. Zhang (2007), An analysis of the scale heights in the lower topside ionosphere based on the Arecibo incoherent scatter radar measurements, *J. Geophys. Res.*, *112*, A06307, doi:10.1029/2007JA012250.

Liu, L., M. He, W. Wan, and M.-L. Zhang (2008), Topside ionospheric scale heights retrieved from Constellation Observing System for Meteorology, Ionosphere, and Climate radio occultation measurements, *J. Geophys. Res.*, *113*, A10304, doi:10.1029/2008JA013490.

Lomb, N. R. (1976), Least-squares frequency analysis of unequally spaced data, *Astrophys. Space Sci.*, *39*(2), 447–462, doi:10.1007/BF00648343.

Mallis, M., and E. Essex (1993), Diurnal and seasonal variability of the southern-hemisphere main ionospheric trough from differential-phase measurements, *J. Atmos. Terr. Phys.*, *55*(7), 1021–1037, doi:10.1016/0021-9169(93)90095-G.

Moffett, R., and S. Quegan (1983), The mid-latitude trough in the electron concentration of the ionospheric F-layer: A review of observations and modelling, *J. Atmos. Terr. Phys.*, *45*(5), 315–343, doi:10.1016/S0021-9169(83)80038-5.

Nishida, A. (1967), Average structure and storm-time change of the polar topside ionosphere at sunspot minimum, *J. Geophys. Res.*, *72*(23), 6051–6061, doi:10.1029/JZ072i023p06051.

Pedatella, N. M., and K. M. Larson (2010), Routine determination of the plasmapause based on COSMIC GPS total electron content observations of the midlatitude trough, *J. Geophys. Res.*, *115*, A09301, doi:10.1029/2010JA015265.

Pedatella, N. M., J. Lei, J. P. Thayer, and J. M. Forbes (2010), Ionosphere response to recurrent geomagnetic activity: Local time dependency, *J. Geophys. Res.*, *115*, A02301, doi:10.1029/2009JA014712.

Pintér, B., S. Thom, R. Balthazor, H. Vo, and G. Bailey (2006), Modeling subauroral polarization streams equatorward of the plasmapause footprints, *J. Geophys. Res.*, *111*, A10306, doi:10.1029/2005JA011457.

Pirog, O. M., N. M. Polekh, E. B. Romanova, A. V. Tashchilin, and G. A. Zherebtsov (2009), The main ionospheric trough in the East Asian region: Observation and modeling, *J. Atmos. Sol. Terr. Phys.*, *71*(1), 49–60, doi:10.1016/j.jastp.2008.10.010.

Prölss, G. (1995), Ionospheric *F* region storms, in *Handbook of Atmospheric Electrodynamics*, vol. 2, pp. 195–248, CRC Press, Boca Raton, Fla.

Prölss, G. W. (2007), The equatorward wall of the subauroral trough in the afternoon/evening sector, *Ann. Geophys.*, *25*(3), 645–659, doi:10.5194/angeo-25-645-2007.

Prölss, G. W., and M. Ocko (2000), Propagation of upper atmospheric storm effects towards lower latitudes, *Adv. Space Res.*, *26*(1), 131–135, doi:10.1016/S0273-1177(99)01039-X.

Pryse, S. E., L. Kersley, M. J. Williams, and I. K. Walker (1998), The spatial structure of the dayside ionospheric trough, *Ann. Geophys.*, *16*(10), 1169–1179, doi:10.1007/s00585-998-1169-4.

Pryse, S. E., L. Kersley, D. Malan, and G. J. Bishop (2006), Parameterization of the main ionospheric trough in the European sector, *Radio Sci.*, *41*, RS5S14, doi:10.1029/2005RS003364.

Rino, C., R. Livingston, R. Tsunoda, R. Robinson, J. Vickrey, C. Senior, M. Cousins, J. Owen, and J. Klobuchar (1983), Recent studies of the structure and morphology of auroral zone *F* region irregularities, *Radio Sci.*, *18*(6), 1167–1180, doi:10.1029/RS018i006p01167.

Rishbeth, H. (1967), The effect of winds on the ionospheric *F*2-peak, *J. Atmos. Terr. Phys.*, *29*(3), 225–238, doi:10.1016/0021-9169(67)90192-4.

Rishbeth, H. (1968), The effect of winds on the ionospheric *F*2-peak–II, *J. Atmos. Terr. Phys.*, *30*(1), 63–71, doi:10.1016/0021-9169(68)90041-X.

Rishbeth, H., and O. K. Garriott (1969), *Introduction to Ionospheric Physics*, Academic, San Diego, Calif.

Rocken, C., K. Ying-Hwa, W. Schreiner, D. Hunt, S. Sokolovskiy, and C. McCormick (2000), COSMIC system description, *Terr. Atmos. Oceanic Sci.*, *11*(1), 21–52.

Rodger, A. (2008), The Mid-latitude Trough: Revisited, in *Midlatitude Ionospheric Dynamics and Disturbances*, *Geophys. Monogr. Ser.*, vol. 181, edited by P. M. Kintner Jr. et al., pp. 25–33, AGU, Washington, D.C.

Rodger, A. S., L. H. Brace, W. R. Hoegy, and J. D. Winningham (1986), The poleward edge of the mid-latitude trough: Its formation, orientation and dynamics, *J. Atmos. Terr. Phys.*, *48*(8), 715–728, doi:10.1016/0021-9169(86)90021-8.

Rodger, A., R. Moffett, and S. Quegan (1992), The role of ion drift in the formation of ionisation troughs in the mid- and high-latitude ionosphere: A review, *J. Atmos. Terr. Phys.*, *54*(1), 1–30, doi:10.1016/0021-9169(92)90082-V.

Rycroft, M. J., and S. J. Burnell (1970), Statistical analysis of movements of the ionospheric trough and the plasmapause, *J. Geophys. Res.*, *75*(28), 5600–5604, doi:10.1029/JA075i028p05600.

Rycroft, M. J., and J. O. Thomas (1970), The magnetospheric plasmapause and the electron density trough at the Alouette I orbit, *Planet. Space Sci.*, *18*(1), 65–80, doi:10.1016/0032-0633(70)90067-X.

Scali, J. L. (1992), *The Mid-Latitude Trough: A Review*, Lowell Cent. for Atmos. Res., Mass. Univ., Lowell.

Schreiner, W., C. Rocken, S. Sokolovskiy, S. Syndergaard, and D. Hunt (2007), Estimates of the precision of GPS radio occultations from the COSMIC/FORMOSAT-3 mission, *Geophys. Res. Lett.*, *34*, L04808, doi:10.1029/2006GL027557.

Schunk, R. W., and P. M. Banks (1975), Auroral N_2 vibrational excitation and the electron density trough, *Geophys. Res. Lett.*, *2*(6), 239–242, doi:10.1029/GL002i006p00239.

Schunk, R. W., W. J. Raitt, and P. M. Banks (1975), Effect of electric fields on the daytime high-latitude *E* and *F* regions, *J. Geophys. Res.*, *80*(22), 3121–3130, doi:10.1029/JA080i022p03121.

Sharp, G. W. (1966), Midlatitude trough in the night ionosphere, *J. Geophys. Res.*, *71*(5), 1345–1356, doi:10.1029/JZ071i005p01345.

Sojka, J. J., and R. W. Schunk (1989), Theoretical study of the seasonal behavior of the global ionosphere at solar maximum, *J. Geophys. Res.*, *94*(A6), 6739–6749, doi:10.1029/JA094iA06p06739.

Sojka, J. J., W. J. Raitt, and R. W. Schunk (1981), Plasma density features associated with strong convection in the winter high-latitude *F* region, *J. Geophys. Res.*, *86*(A8), 6908–6916, doi:10.1029/JA086iA08p06908.

Spiro, R. W. (1978), A study of plasma flow in the mid-latitude ionization trough, Ph.D. dissertation, Texas Univ., Dallas.

Spiro, R. W., R. A. Heelis, and W. B. Hanson (1978), Ion convection and the formation of the mid-latitude *F* region ionization trough, *J. Geophys. Res.*, *83*(A9), 4255–4264, doi:10.1029/JA083iA09p04255.

Spiro, R., R. Heelis, and W. Hanson (1979), Rapid subauroral ion drifts observed by Atmosphere Explorer C, *Geophys. Res. Lett.*, *6*(8), 657–660, doi:10.1029/GL006i008p00657.

St.-Maurice, J. P., and D. G. Torr (1978), Nonthermal rate coefficients in the ionosphere: The reactions of O+ with N_2, O_2, and NO, *J. Geophys. Res.*, *83*(A3), 969–977, doi:10.1029/JA083iA03p00969.

Temmer, M., B. Vršnak, and A. Veronig (2007), Periodic appearance of coronal holes and the related variation of solar wind parameters, *Sol. Phys.*, *241*(2), 371–383, doi:10.1007/s11207-007-0336-1.

Titheridge, J. E. (1995), Winds in the ionosphere: A review, *J. Atmos. Terr. Phys.*, *57*(14), 1681–1714, doi:10.1016/0021-9169(95)00091-F.

Tsurutani, B. T., W. D. Gonzalez, A. L. C. Gonzalez, F. Tang, J. K. Arballo, and M. Okada (1995), Interplanetary origin of geomagnetic activity in the declining phase of the solar cycle, *J. Geophys. Res.*, *100*(A11), 21,717–21,733, doi:10.1029/95JA01476.

Tsurutani, B. T., et al. (2006), Corotating solar wind streams and recurrent geomagnetic activity: A review, *J. Geophys. Res.*, *111*, A07S01, doi:10.1029/2005JA011273.

Turunen, T., and L. Liszka (1972), Comparison of simultaneous satellite measurements of auroral particle precipitation with bottomside ionosonde measurements of the electron density in the *F* region, *J. Atmos. Terr. Phys.*, *34*(3), 365–372, doi:10.1016/0021-9169(72)90039-6.

Voiculescu, M., and T. Nygrén (2007), IMF effect on ionospheric trough occurrence at equinoxes, *Adv. Space Res.*, *40*(12), 1935–1940, doi:10.1016/j.asr.2007.04.108.

Voiculescu, M., I. Virtanen, and T. Nygrén (2006), The *F* region trough: Seasonal morphology and relation to interplanetary magnetic field, *Ann. Geophys.*, *24*(1), 173–185, doi:10.5194/angeo-24-173-2006.

Voiculescu, M., T. Nygrén, A. Aikio, and R. Kuula (2010), An olden but golden EISCAT observation of a quiet-time ionospheric trough, *J. Geophys. Res.*, *115*, A10315, doi:10.1029/2010JA015557.

Wan, W., L. Liu, X. Pi, M. L. Zhang, B. Ning, J. Xiong, and F. Ding (2008), Wavenumber-4 patterns of the total electron content over the low latitude ionosphere, *Geophys. Res. Lett.*, *35*, L12104, doi:10.1029/2008GL033755.

Werner, S., and G. W. Prölss (1997), The position of the ionospheric trough as a function of local time and magnetic activity, *Adv. Space Res.*, *20*(9), 1717–1722, doi:10.1016/S0273-1177(97)00578-4.

Whalen, J. A. (1989), The daytime *F* layer trough and its relation to ionospheric-magnetospheric convection, *J. Geophys. Res.*, *94*(A12), 17,169–17,184, doi:10.1029/JA094iA12p17169.

Wielgosz, P., L. W. Baran, I. I. Shagimuratov, and M. V. Aleshnikova (2004), Latitudinal variations of TEC over Europe obtained from GPS observations, *Ann. Geophys.*, *22*(2), 405–415, doi:10.5194/angeo-22-405-2004.

Yizengaw, E., and M. Moldwin (2005), The altitude extension of the mid-latitude trough and its correlation with plasmapause position, *Geophys. Res. Lett.*, *32*, L09105, doi:10.1029/2005GL022854.

Yizengaw, E., H. Wei, M. Moldwin, D. Galvan, L. Mandrake, A. Mannucci, and X. Pi (2005), The correlation between mid-latitude trough and the plasmapause, *Geophys. Res. Lett.*, *32*, L10102, doi:10.1029/2005GL022954.

Yue, X., W. S. Schreiner, J. Lei, S. V. Sokolovskiy, C. Rocken, D. C. Hunt, and Y. H. Kuo (2010), Error analysis of Abel retrieved electron density profiles from radio occultation measurements, *Ann. Geophys.*, *28*(1), 217–222, doi:10.5194/angeo-28-217-2010.

M. He, L. Liu (corresponding author), W. Wan, and B. Zhao, Beijing National Observatory of Space Environment, Institute of Geology and Geophysics, Chinese Academy of Sciences, Beijing 100029, China. (hems@mail.igcas.ac.cn; liul@mail.igcas.ac.cn; wanw@mail.igcas.ac.cn; zbqjz@mail.igcas.ac.cn)